Flux Weakening Control of Electric Starter-Generator Based on Permanent-Magnet Machine

Serhiy Bozhko, *Member, IEEE,* Mohamed Rashed, Christopher Ian Hill, *Member, IEEE,* Seang Shen Yeoh, and Tao Yang

***Abstract*— The paper presents control analysis and design for a Permanent Magnet Machine (PMM) operated in Flux-Weakening (FW) mode for an aircraft electric starter-generator application. Previous literature has focused on FW control of PMMs in motoring (starting) mode, however the system stability and control in generating mode has been inadequately studied. The paper reports detailed, rigorous control analysis and design for a PMM based aircraft electric starter-generator operated in flux-weakening mode. It is shown that an unstable area of operation exists. A novel control scheme which eliminates this instability is proposed. The key analytical findings of the paper are verified by experimental investigation. The paper therefore concludes that the presented technique is able to ensure system stability under all modes of operation. Furthermore, it is noted that the findings of this work are also valuable for any two-quadrant PMM drive with frequent change between starting and generating regimes under current-limiting operation.**

***Index Terms*— Permanent magnet machines, Generators, Stability, Current control, Limiting.**

I. Introduction

Many aircraft system technologies are undergoing major changes due to a global tendency towards environmentally responsible air transportation. The state-of-the art on-board systems are expected to be more efficient, very safe, simpler in servicing and easier in maintenance [1] - [3]. As a result, many existing hydraulic and pneumatic power driven systems are being replaced by their electrical counterparts. This trend is known as a move towards the "more electric aircraft" (MEA) and results in an increased number of newly introduced electrical loads to power many primary functions including actuation, de-icing and anti-icing, cabin air-conditioning, and engine start [2], [4]. Hence, the total on-board electric power budget is substantially increased. Therefore, electric power generation systems have a key role in supporting this technological trend. The aim is to reduce weight, increase efficiency hence reduce fuel burn. New systems in MEA are often designed to integrate different functions. A good example of this is integration of engine starting, previously implemented by pneumatic energy, with electric generation. Both these functions can now be performed by integrated electric starter-generator (SG) system.

The stat-of-the-art starter-generator technology employs a three-stage wound-field synchronous machine. However, performing a starter function requires an additional winding hence compromising the overall system weight and adding complexity to the machine. Nowadays, advances in modern power electronics allow the developers to consider novel machine types for application as SG. Potentially, this will result in substantial improvements in power density (kW/kg) and in overall system performance. Many potential topologies are under investigation [5], [6], [7]. In the case of PMMs, as utilised in this study, the constant rotor flux of the PMM does impose safety concerns during ab-normal operating situations such as converter switch off and the engine speed overshooting the machine's maximum operating speed. However, there are possible solutions that can be adopted to handle this drawback of the PMM technology. The first solution is to disconnect the PMM electrical terminals from the converter, while in the second the converter is used to apply a short circuit to the PMM terminals. In the case of the short circuit solution, the PMM/converter should be designed so that the short circuit current is less than the maximum current limit. This paper deals with one of the possible topologies based on a permanent magnet machine (PMM) controlled by active front-end rectified (AFE), as illustrated by Fig. 1.

.

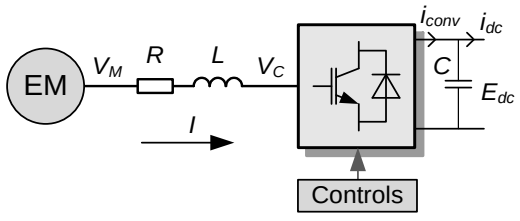

Fig. 1. Topology of SG system based on PMM fed by AFE

In order to implement the electrical engine start, the SG system in motoring mode is required to cover the worst-case (typically corresponding to cold conditions at -40°C) envelope of engine

Authors affiliations and contact details:
Serhiy Bozhko, Mohamed Rashed, Cristopher Ian Hill, Seang Shen Yeoh, and Tao Yang are with the Power Electronics, Machine and Control Group, University of Nottingham, Nottingham NG2 7SP, United Kingdom (serhiy.bozhko@nottingham.ac.uk, mohamed.rashed@nottingham.ac.uk, c.hill@nottingham.ac.uk, seang.yeoh@nottingham.ac.uk, and tao.yang@nottingham.ac.uk)

torque-speed characteristics (example is given in Fig. 2) in order to ensure safe and quick engine start. Hence, a SG drive system will provide engine acceleration up to the point that the engine reaches a self-sustaining speed. In some cases it may be requested to continue operation in motoring mode even beyond, as engine and starter combined will reach ground idle speed much faster. As the engine speed reaches a lower generation speed value, the system turns into generation mode off-taking mechanical power from the engine, converting it into an electrical power and supplying it into the grid [5].

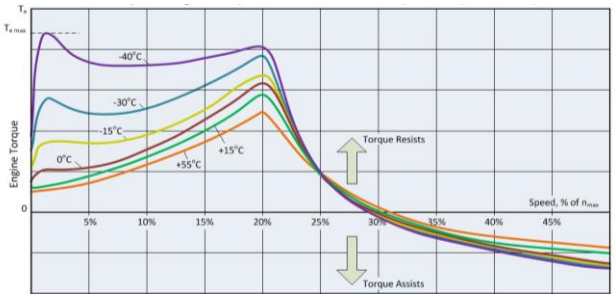

Fig. 2. Example of engine torque curves vs ambient temperature at sea level

The design of the SG system should include coordinated consideration of machine-converter interactions. For instance, the SG operation should be optimized for generation mode, since a vast proportion of the exploitation time it is operated in generation mode. In general, the converter must therefore be able to deal with high speeds and associated large voltages. However the same converter must also be able to handle starting mode; this is associated with high torque hence with high current. Overall, it means that the converter kVA rating should be selected according to point A in Fig. 3. Unfortunately, this will mean that the converter will be significantly underutilised under normal operating conditions and hence cannot be considered optimized. Furthermore, the converter kVA rating will basically define the weight and volume of the converter (crucial for aircraft applications) as well as its cost and so this oversizing is a serious problem. These can be reduced to some extend by moving the machine electromagnetic design point down the saturation curve, however this will increase the size, and hence the weight, of the machine [5]. A better solution would be to introduce a reconfigurable winding, for example, switching from series to parallel configuration, depending on an operational mode (for example, selecting point B or C in Fig. 3 for the design). However, this will lead to an increased number of switches, increased converter kVA rating and less efficiency due to additional losses in devices [5].

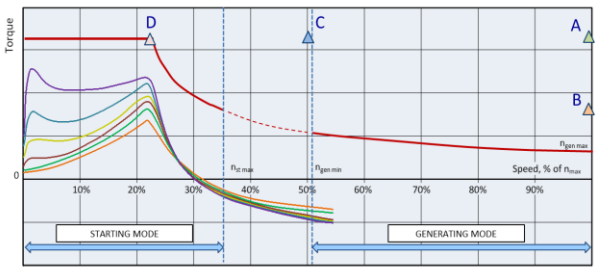

Fig. 3. Torque-speed requirements of SG system

Another option is to operate the machine in a flux weakening (FW) mode [8]. In this case when above a certain speed ("base" speed, illustrated by point D in Fig. 3) the machine flux is gradually reduced thus limiting the machine stator voltage. This means that the converter voltage rating can be significantly reduced. Therefore, employment of FW control brings important benefits for future aircraft SG system, since the dc-link voltage in MEA EPS is typically low (270V). This is low compared to the induced EMF in practical high-speed machine design.

During the development of the PMM-AFE based SG system controller, detailed in this paper, the authors have found that rigorous FW control design for PMMs operated in generation mode has not been adequately presented in known publications. Our study addresses this gap and the key findings are reported below in this paper. The results may be of interest not only for SG developers but for a wider community dealing with advanced control of PMM-based drives.

Flux weakening is achieved by controlling the "flux current component" i_d which creates opposite flux to the permanent magnet flux and hence reduces the machine back EMF. This enables operation at higher speeds while maintaining a fixed output voltage from the converter to the PMM. There are many control strategies presented within literature for FW of PMM. Among them is the voltage magnitude control strategy, in which the stator voltage magnitude is regulated to track the maximum output voltage from the converter via controlling i_d. This method was investigated in [8] - [14] where i_d is directly controlled by the voltage controller that gives the reference d-axis current $i_{d\text{-ref}}$ while the torque reference current component $i_{q\text{-ref}}$ is dynamically limited in order to satisfy the current limit I_{max}. I_{max} is normally set to achieve some control goals e.g. maximum torque-per-ampere capability as in [8] or set to control the PMM speed, [10]. The voltage magnitude controller is also used to provide the phase angle of the PMM reference current vector as in [15], [16]. In [15], [16] an adaptive voltage magnitude controller is designed and voltage control stability analysis is performed for motoring mode only. In [13], the plant for FW controller is derived for PMM drive systems. The derivation is done for motoring mode, and takes into consideration the feedforward terms and current loop dynamics. The stability of the FW controller is analysed using Routh-Hurwitz criterion and the stability range is illustrated with the help of the current and voltage limit circles. Further analysis showed small values (or none) of proportional gain yield better stability results. This is supported by findings from [5].

A new FW control scheme for PMM drives was proposed by [17]. The control scheme was designed to operate under non-FW and FW (including full load) situations for motoring mode only. The experimental results validate the new FW control scheme, showing robust speed control while achieving high efficiency performance. Another FW voltage control approach is presented in [18], [19]. In this approach, the voltage angle is determined by a single current controller, either i_d or i_q, while the voltage magnitude is set to the maximum output value from the converter. In [19], the d-axis current controller is used for motoring mode and the voltage control loop is switched to the q-axis current controller in generating mode. The current limit I_{max} is regulated by the speed controller. The main

drawbacks of this FW control approach are weak stability and the requirement of transition mechanisms to change the control loop between constant torque and FW [18]; also between motoring and generating modes in FW. In [18], modifications to the control strategy presented in [19] are proposed to improve the system stability and to achieve smoother transition between the operating modes.

In [20], the model based design of the FW controller was investigated in motoring mode only. It was discovered that the derived linear plant was non-minimum phase and the FW controller would have limited stability. The FW control is applied by means of controlling the voltage phase of the PMM by injecting negative i_d. Based on the control scheme, the analytical function of the positive zero that characterise the plant non-minimum phase was also derived. Experimental results showed the effectiveness of the control scheme. The FW control approach was derived based on the operating regions between the voltage and current limit circles in [21]. The different parts of the FW regions are identified analytically and they are used in the control scheme. This enables FW control for both finite and infinite constant power speed ratio surface mounted type PMM. The control scheme has been verified with simulation analysis and experimental tests for motoring mode only.

In literature, the flux weakening control systems reviewed above were mostly investigated (for stability and control design) for the motoring mode, there are very few reports on the design or stability analysis of the voltage control loop in generating and current limiting mode. Even when the paper investigated a control scheme in generator mode, it usually just covers the feasibility and control concept. In [22], the influence of stator resistive drop, saturation, cross coupling, magnet flux-linkage, and DC bus voltage on the PMM drive system within the Constant Power Speed Range (CPSR) is investigated. The variations affect the stability range shown in voltage and current limit circles plus MTPA trajectories. The presented results revealed that the stator resistance and DC bus voltage led to a difference in the speed range within the constant power region. The other factors only changed the shape of the circles and trajectories. In [23], a FW control scheme is introduced for IPM S/G systems. Torque control is applied when operating in motoring mode, while DC link voltage is used in generating mode. The current angle determines the vector i_d and i_q references for the inner current loop controllers. The FW is based on stator current angle strategy which regulates the AC magnitude voltage. Simulation and experimental results demonstrated good control performance for both operating modes. In [24], a control strategy is proposed to determine the appropriate control output for either constant torque or constant power region for IPM drive systems. The control scheme is able to provide either MTPA or FW depending on the operation and ensure smooth transition between both control modes. Motoring and regenerative braking were considered for analysis with this control scheme. The proposed control was proven feasible by experimental results. In [25], a robust FW strategy is proposed for SPM drive systems. The FW controller is based on voltage magnitude method with an adaptive controller to achieve both fast dynamic response and minimum copper loss for the whole operating range. The FW control also takes into account stator resistance which is crucial to achieve fast control response. Within this study the resistance of the PMM used for obtaining the experimental results is not small compared to the Xd and Xq values. This resistance is therefore included into the theoretical analysis. It should be also noted that for high speed PMMs, the stator resistance changes with the operating frequency and it will have significant value at high speeds (i.e. during flux weakening).

In this paper, the FW voltage magnitude control strategy is considered for detailed/rigorous stability analysis and control design with focus on generating and current limiting modes. The merits of the voltage magnitude control strategy are; the smooth transition between the PMM operating modes using single and simple control structure. Operation of a PMM at high speed, with limited DC bus voltage, will require operation in flux-weakening (FW) mode [26] - [27] however rigorous control design for PMMs in generation and FW mode is not presented in known publications. Our paper attempts to fill this gap.

The contributions of this paper are:

1- Detailed stability analysis and control design of the FW based voltage magnitude control of PMM especially in generating and current limiting modes, which are not extensively investigated in the literature.
2- Unstable operating areas in generating mode of voltage control are identified.
3- New modified current limiting model is proposed and adaptive voltage controller is designed to stabilize the control system in generating mode.
4- Experimental validation and investigation of the reported stability analysis and of the proposed control design approach.

The paper is organised into six sections. Section II details the PMM-AFE system as a plant and FW control scheme. Small-signal analysis of the FW control loop is presented in Section III. Based on this, the machine voltage controller (or FW controller) is presented in Section IV. The novel current limiting method to eliminate the area of instability is detailed in Section V. Simulation results are presented in Section VI. Experimental validation of the system performance and stability analysis is given in Section VII. Finally, the overall conclusions of the paper are summarised.

II. Plant of Control

The plant of control includes a PMM fed by an AFE. The control analysis and design have been conducted using standard PMM models in the synchronously rotating *dq* reference frame with the *d*-axis aligned with the machine rotor [8], [26]:

$$L_d \frac{di_d}{dt} = -R_s i_d + \omega_{re} L_q i_q + v_d \tag{1}$$

$$L_q \frac{di_q}{dt} = -R_s i_q - \omega_{re} L_d i_d - \omega_{re} \psi_r + v_q \tag{2}$$

where: v_d, v_q, i_d and i_q are the *d* and *q*-axis voltage and current components, R_s, L_d and L_q are the stator resistance and inductances, ω_r is the mechanical speed, ω_{re} is electrical rotor speeds ($\omega_{re} = p\omega_r$), ψ_r is the permanent magnet flux, K_m is the machine constant, $K_m = 3p/2$ and p is the PMM number of pole pairs.

In starting mode, the controlled variable is the machine speed, this is governed by the following expression:

$$J\frac{d\omega_r}{dt} = T - T_l = K_m\left[\psi_r i_q + \left(L_d - L_q\right)i_d i_q\right] - T_l \tag{3}$$

where J is the system inertia and T_l is the load torque.

In generating mode, the controlled variable, according to the designed system requirements, is the output dc current. For the selected converter topology this can be governed by the converter non-switching model as follows [28]:

$$i_{dc} = \frac{\sqrt{3}}{2}\left(m_d i_d + m_q i_q\right) \tag{4}$$

Here, m_d and m_q are the modulation indexes of the converter:

$$m_d = \frac{v_d}{E_{dc}/\sqrt{3}},\quad m_q = \frac{v_q}{E_{dc}/\sqrt{3}} \tag{5}$$

where E_{dc} is the converter output voltage (across the output capacitor C):

$$C\frac{dE_{dc}}{dt} = i_{conv} - i_{dc} \tag{6}$$

In (6), i_{conv} is the converter DC side current and i_{dc} is the current drawn by the load. This is shown in

Fig. 1.

Equations (1)-(6) govern the controlled plant and form the basis of the control design reported below.

Typically, the PMM operation is limited by the maximum output current and voltage from the converter. These limits are implemented in the control system as follows:

- The stator voltage magnitude V_s is controlled to the reference value V_s^* defined by the converter output voltage, or in case of aircraft EPS, by dc-bus voltage (typically 270V for MEA). In the studied control system, the stator voltage control is performed by flux weakening (at speeds exceeding the machine base speed) injecting a negative flux current component i_d , hence the converter over-modulation is avoided. The machine stator voltage V_s is given by the equation:

$$V_s = \sqrt{v_d^2 + v_q^2} \tag{7}$$

- the machine current is limited to $I_{\max}$:

$$\sqrt{i_d^2 + i_q^2} \le I_{\max} \tag{8}$$

- the operating speed range of the SG system does not require maximum torque per voltage (MTPV), hence it is not covered in this paper.

It follows from (8) that the available i_q resource reduces with increasing machine speed as more i_d will be required in order to de-flux the machine and satisfy (7).

The overall control system is built using classical cascaded control loops, as depicted in

Fig. 4. The internal loops provide decoupled *d*- and *q*- current control using standard proportional-integral (PI) controllers designed for a closed-loop bandwidth of 400 Hz and damping factor ζ=0.95. In FW mode, the outer voltage control loop provides the negative reference for i_d control. The i_q reference is produced either by outer speed controller in starting (motoring) mode or by I_{dc} controller in generating mode (these controllers are not detailed here since they are out of the scope of this study). The reference i_q^* comes from the current limiting block, in order to satisfy (8). The reference currents, i_d^* and i_q^* are fed to the "decoupled d- and q-axis current control" box that includes the d and q-axis PI current controllers, arranged with decoupling terms in order to ensure independent control of id and iq current components. The outputs of the box are the reference voltage components v_d^* and v_d^*. Depending on this reference, two modes of operation are possible, namely *limited i_q mode* (LM) and *unlimited i_q mode* (UM). In the LM, a current limiter defines the i_q^* setting based on the values of I_{max} and i_d^*. In the UM, i_q^* is defined by the outer control loop. V_c is the converter output voltage, m_{abc} is the modulation index for phases abc and θ_r is the rotor position.

This study aims to provide a solution for an extended speed range SG system for a business jet; machine and converter parameters of the targeted system are given in Appendix I. Experimental verification of the analytical findings have been conducted using smaller machine-converter system, the parameters of this system are detailed in Appendix II. The numerical calculations in this paper are therefore performed for this smaller mock-up system and the most significant results are also calculated for the business jet parameters.

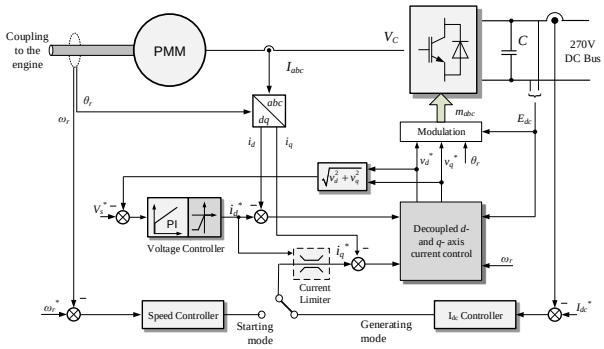

Fig. 4. The control system studied.

III. Flux-Weakening Control Loop Analysis

As discussed in previous section, the machine torque is regulated by setting i_q^* such that the maximum current limit $I_{\max}$ (8) is not violated. If the required stator current magnitude is high, priority is given to i_d^* hence the system goes into LM and i_q^* is limited by the current limiter:

$$i_q^* \le \sqrt{I_{max}^2 - i_d^{*2}} \tag{9}$$

When current limitation is activated (LM mode), i_q follows the reference value calculated by (9) hence depends on i_d^*. In this mode, i_d^* alone defines the active and reactive powers provided to the PMM by the converter. In this section, the two current control modes (UM and LM) will be analysed in detail.

A. Voltage Control Loop in Unlimited i_q Mode

The voltage control loop includes a nonlinear term (7) in the feedback; therefore linearization is required for small signal analysis and subsequent control design. The small-signal model for (7) can be derived as:

$$\Delta V_s = \frac{v_{d0}}{V_{s0}}\Delta v_d + \frac{v_{q0}}{V_{s0}}\Delta v_q \tag{10}$$

where variables indexed with zero denote their steady-state value around the selected linearization point, and

$$\Delta v_d = \left(R_s + L_d s\right)\Delta i_d - \omega_{re0} L_q \Delta i_q - i_{q0} L_q \Delta\omega_{re} \quad (11)$$

$$\Delta v_q = \left(R_s + L_q s\right)\Delta i_q + \omega_{re0} L_d \Delta i_d + \left(i_{d0} L_d + \psi_r\right)\Delta\omega_{re} \quad (12)$$

Here $\Delta\omega_{re}$ is derived according to the mechanical equation (3) as:

$$Js\Delta\omega_r = K_m\left(\psi_r \Delta i_q + \left(L_d - L_q\right)\left(i_{d0}\Delta i_q + i_{q0}\Delta i_d\right)\right) + T_{l0}\Delta\omega_r,$$

$$T_{l0} = \frac{\partial T_L}{\partial \omega_r} \quad (13)$$

According to the control paradigm of controlling the voltage by *d*-axis current, using (10)-(13) and considering i_q and ω_{re} as disturbances, one can derive the small-signal open-loop transfer function of interest as follows:

$$\frac{\Delta V_s}{\Delta i_d}(s) = \frac{1}{V_{s0}} \cdot \frac{a_2 s^2 + a_1 s + a_0}{b_1 s + b_0} \quad (14)$$

Polynomial coefficients in (14) depend on the selected operational point for linearization and their analytical expressions are given in Appendix III. As one can see, the plant (14) has two zeros and one pole. For the particular cases of machine with surface-mounted magnets (SPMM, for which $L_d = L_q$), or if the machine is driven by constant speed ($\omega_r = const$ or $J \to \infty$), the plant (14) can be further reduced:

$$\frac{\Delta V_s}{\Delta i_d}(s) = \frac{1}{V_{s0}} \cdot \left(L_d v_{d0} s + \left(R_s v_{d0} + L_d v_{q0} \omega_{re0}\right)\right) \quad (15)$$

In this case the plant of control is represented by single zero. Based on the practical assumption that the mechanical time response of the PMM is typically much slower than that of the electrical system (this assumption is widely adopted and employed in literature, for example in [15], [16], [18]), for the purpose of voltage control loop design, the machine speed ω_r in this study is assumed to be constant. This will justify the control plant model (15) for interior-magnet PMM with $L_d \neq L_q$ as well. From (15) the value of the plant zero can be derived as follows:

$$z_{pl1} = -\frac{R_s v_{d0} + L_d v_{q0} \omega_{re0}}{L_d v_{d0}} \quad (16)$$

Analysing (16) one can conclude that the plant zero changes its value (i.e. location in complex plane) with the change of the machine operational point. From (16), there is a break-up point at $v_{d0} = 0$, when $z_{pl1}=\infty$. This point corresponds to the border between the generation and starting modes. Hence, in generating mode the zero is negative, hence located in the left-hand part of the complex s-plane, and in motoring mode it is located in the right-hand side of the semiplane. This means that in motoring mode the voltage control loop is a non-minimum phase, therefore careful control design is required in order to keep the system closed-loop poles on the left-hand side of the s-plane. The break-up points condition can be derived analytically from (11):

$$i_{q0} = \frac{R_s}{\omega_{re0} L_q} i_{d0} \quad (17)$$

The movement of the plant zero is illustrated for the machine and converter detailed in Appendix II. The values of the zero were calculated for varying i_q; assuming flux-weakening operation, within a speed range of 3600-4000rpm, with V_s = 250V, including motoring (i_q>0) and generating (i_q<0) modes. The trajectories of the zero are plotted in Fig. 5.

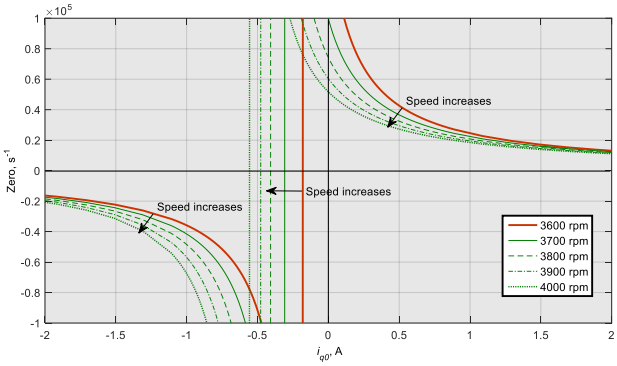

Fig. 5. Trajectory of zero in (15) for UM at V_s =250V.

The small signal model of the voltage control loop can be depicted by the block diagram shown in Fig. 6. In addition to the plant (15), the control loop includes a voltage controller of transfer function $G_V(s)$ and the i_d -current control loop represented by closed loop transfer function $G_{id}(s)$. Based on the analysis above, the voltage controller design should be performed assuming the worst-case scenario, namely, for starting mode (i.e. non-minimum phase case) with large i_{q0} (when the plant zero is close to the origin and nearly independent of the motor speed). The resultant voltage controller design is also expected to provide superior control performance in generating mode when the plant becomes minimum-phase.

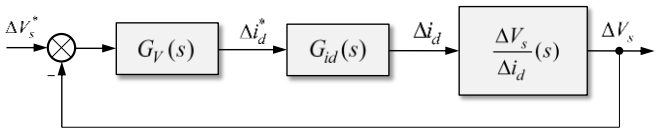

Fig. 6. Small-signal voltage control loop block-diagram

The control design is illustrated below using mock-up system parameters of Appendix II. First, the operational point V_s = 250V, i_{q0}=8A, $\omega_{re0}=2\pi\cdot 3600.p/60$ is selected (p=3). Then, the open loop poles and zeros of the extended plant (i.e. plant (15) combined with the i_d-current control loop as shown in Fig. 6) are calculated and their positions on the s-plane are examined (summary is given in Table I and illustrated by Fig. 7). The extended plant has two open loop zeros and two open loop poles: one zero (z_1) is according to (15), another one (z_2) is of the controller $G_V(s)$ and the two poles $p_{1,2}$ of the current control loop $G_{id}(s)$. These are listed in Table I; the corresponding root locus is given in Fig. 7.

TABLE I. ZEROS AND POLES OF THE VOLTAGE CONTROL PLANT (I_{Q0} = 8A, 3600RPM, V_S=250V)

z_1	z_2	$p_{1,2}$
3132.2	-686.2	-1128.8±362.3i

The zero z_1 is on the right side of the s-plane and both z_2 and $p_{1,2}$ are on the left side. Based on the positions of z_1, z_2 and $p_{1,2}$, it is found sufficient to use only an integral voltage controller for such a non-minimum phase control system. The corresponding root locus is given in Fig. 7. In the considered case the voltage control loop is stable if the integral controller gain k_{iv} does not exceed 396. The voltage controller gain is then selected as k_{iv}=100 to be marginally less than the maximum value without compromising the system dynamic performance. The closed-loop poles at k_{iv}=100 are marked by red crosses in Fig. 7. For generating mode, k_{iv} can be selected as high as possible since the voltage control loop is a minimum phase system, however the selected k_{iv} value (which is designed for motoring mode) delivers good performance and is used for operation in both generating and motoring modes in UM.

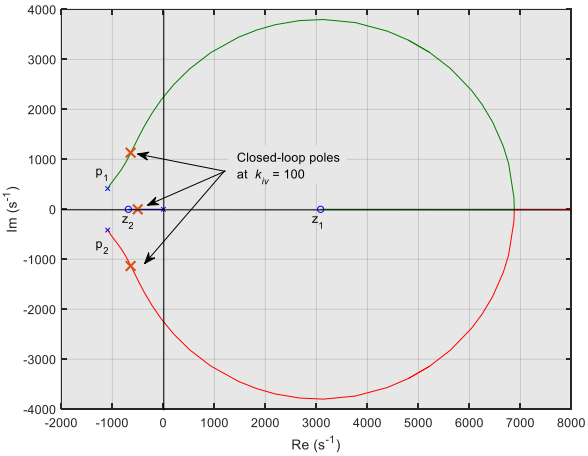

Fig. 7. Root locus of the voltage control loop with integral voltage controller in UM (i_{q0} = 8A, 3600rpm, V_s=250V).

B. Voltage Control Loop in Limited i_q Mode

When the PMM is operated in flux weakening and a large torque is required (either in motoring or in generating mode), a dynamic limitation of i_q^* can occur and the system goes into LM operation (this may happen, for example, if full-torque acceleration is required in motoring mode under flux weakening). As soon as the machine speed goes above the base value (at which system enters into flux weakening mode), the value of i_q^* must be reduced to satisfy the condition (9). Hence, in LM, the i_q current loop will not process the output of corresponding outer-loop controller, but the output signal of a nonlinear block (9) instead. The following small-signal model for i_q^* can be established:

$$\Delta i_q^* = \frac{-i_d^*}{\sqrt{I_{max}^2 - i_d^{*2}}}\Delta i_d^* \approx -\frac{i_{d0}}{i_{q0}}\Delta i_d^* \tag{18}$$

Using (10) and (18), and following some algebraic manipulations, one can derive the plant of voltage control in the LM:

$$\frac{\Delta V_s}{\Delta i_d}(s) = \frac{1}{i_{q0}V_{s0}} \cdot \frac{a_{2L}s^2 + a_{1L}s + a_{0L}}{b_{1L}s + b_{0L}} \tag{19}$$

Polynomial coefficients in transfer function (19) are dependent on the selected operational point and given in Appendix IV. Assuming, as for UM case above, that the speed is constant and has identical current loops, the plant (19) can be reduced to:

$$\frac{\Delta V_s}{\Delta i_d}(s) = \frac{1}{i_{q0}V_{s0}} \cdot (a_{2L}s + a_{1L}) \tag{20}$$

where $a_{1L} = -i_{d0}\left(R_s v_{q0} - L_q v_{d0}\omega_{re0}\right) + i_{q0}\left(R_s v_{d0} + L_d v_{q0}\omega_{re0}\right)$ and $a_{2L} = L_d i_{q0} v_{d0} - L_q i_{d0} v_{q0}$.

The plant (20) has only one zero, as in UM (15). However, contrary to (15), the zero of (20) is on the right-side of the s-plane in generating mode. As such, the plant of the voltage control loop changes from being minimum phase to non-minimum phase if the system goes from UM to LM. Hence, it is important to consider this effect when designing the voltage controller gain k_{iv}.

For the example machine in Appendix II, the trajectories of the zero of the transfer function in (20) at different operating points are illustrated by Fig. 8. As it can be observed, in generating mode (i_q<0 as speed is always positive for aircraft applications) the positive zero moves towards the origin with decreasing i_q. The pole-zero map for the operating point i_{q0}=1A (0.2pu), 3600rpm, V_s = 250V, and the root locus assuming the voltage control loop tuning is consistent with UM (k_{iv}=100), are depicted in Fig. 9. It is clearly seen that under such conditions the voltage control loop goes unstable.

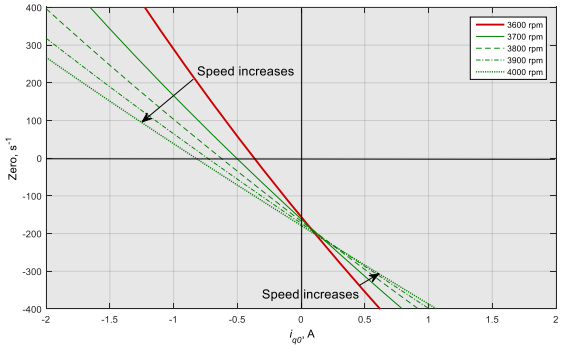

Fig. 8. The trajectory of the zero of the TF $\Delta V_s/\Delta i_d$ (20) for LM.

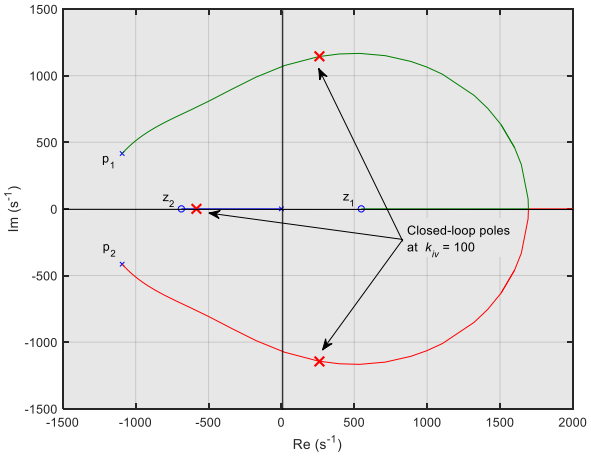

Fig. 9. Root locus of voltage control loop in LM (i_{q0} = -1A, 3600rpm, V_s=250V).

In practice, operation of the system with small i_q^* in LM is a rare practical case. Typically, I_{max} is set according to the maximum current of the power converter controlling the machine and this allows for high $i_{q\text{-}ref}$ values. However, as a result of an external command (under command from supervisory control system, power management control in multi-source EPS etc) I_{max} can be intentionally limited to a small value. In addition, when the engine speed approaches the limit at which the value of the required demagnetising current i_d is very close to the value of I_{max} the permissible value of i_q is small. The example in Fig. 9 demonstrates the non-minimum phase nature of the system, and hence the unstable voltage loop, when I_{max} is limited to 1.64A (0.2pu). Hence, there is a need to use an adaptive k_{iv} gain to match the change in control characteristics of the voltage loop with the change in PMM operational mode.

The next section will investigate the stability boundary limits for k_{iv} under all possible operating points and proposes an adaptive k_{iv} gain design approach.

IV. Voltage Controller Design

The analysis in the previous section shows that stable operation in generation and LM requires adaptive change of k_{iv} according to the variation of the system operating point. As the starting point of such a design, Routh-Hurwitz criterion has been applied to the characteristic equation of the closed voltage control loop in order to determine the stability boundary limits for k_{iv}. From (15) and (20) the plant of voltage control can be expressed as:

$$\frac{\Delta V_s}{\Delta i_d}(s) = K_{pl} \cdot (s + z_{pl}) \tag{21}$$

where K_{pl} and z_{pl} are the plant gain and zero, their values are defined for UM by (15) and for LM by (20). The internal loop of i_d current control under standard tuning [26] is represented by transfer function:

$$G_{id}(s) = \frac{K_i (s + z_i)}{(s + p_{i1})(s + p_{i2})} \tag{22}$$

where its zero z_i and poles $p_{i1,2}$ are defined by the loop tuning criteria. The integral voltage controller is given by:

$$G_V(s) = \frac{k_{iv}}{s} \tag{23}$$

Based on (21) - (23), the characteristic equation of the voltage control loop is derived in the following form:

$$c_3 s^3 + c_2 s^2 + c_1 s^1 + c_0 = 0 \tag{24}$$

where $c_0 = k_{iv} K_i K_{pl} z_i z_{pl}$, $c_1 = p_{i1} p_{i2} - k_{iv} K_i K_{pl} (z_i + z_{pl})$, , $c_2 = k_{iv} K_i K_{pl} - p_{i1} - p_{i2}$, and $c_3 = 1$. According to the Routh-Hurwitz criteria, the system is stable if all coefficients in (24) are strictly positive and $c_2 c_1 > c_3 c_0$. These conditions lead to the following five boundaries for k_{iv} in order to achieve voltage control loop stability:

$$k_{iv} > k_{L1} = \frac{p_{i1} + p_{i2}}{K_i K_{pl}} \tag{25}$$

$$k_{iv} < k_{L2} = \frac{p_{i1} p_{i2}}{K_i K_{pl} (z_i + z_{pl})} \tag{26}$$

$$k_{iv} = k_{L3} = \mathrm{sgn}(K_i K_{pl} z_i z_{pl}) \tag{27}$$

$$k_{iv} < k_{L4} = \frac{1}{2A}(-B - \sqrt{B^2 - 4AC}) \tag{28}$$

$$k_{iv} > k_{L5} = \frac{1}{2A}(-B + \sqrt{B^2 - 4AC}) \tag{29}$$

where $A = -K_i^2 K_{pl}^2 (z_i + z_{pl})$, $C = -(p_{i1} + p_{i2}) p_{i1} p_{i2}$, and $B = K_i K_{pl}((z_i + z_{pl})(p_{i1} + p_{i2}) - z_i z_{pl} + p_{i1} p_{i2})$. These five boundary limits (25)-(29) define the range of the voltage controller gain k_{iv} in order to keep the loop stable. Fig. 10 illustrates these limits calculated for the example machine of Appendix II in LM at speed 3600 rpm.

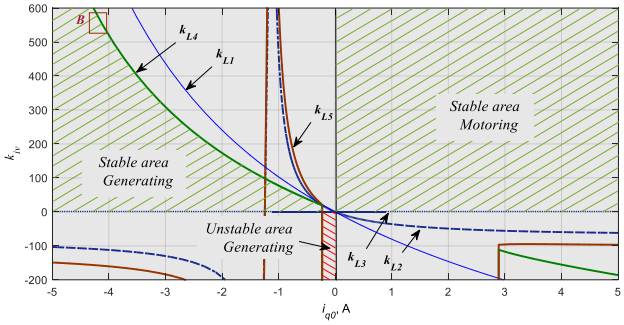

Fig. 10. k_{iv} range for stable LM operation.

As one can clearly see, in motoring mode the voltage control loop is stable for any positive value of k_{iv} (minimum-phase system). In generating mode, the upper value of k_{iv} is limited by the k_{L4} trajectory according to (28). The limit value k_{L4} decreases with decreasing i_q until i_q reaches a critical value at which k_{iv} has to be changed to a negative value to maintain stable operation. At this critical i_q value the plant zero changes its sign (trajectory in Fig. 8 crosses the horizontal axis). The value of i_q at this point can be found from (20) by solving a_1=0, this leads to a quadratic equation. A simplified solution can be derived assuming small enough saliency of the machine, i.e. allowing replacement of L_d and L_q by the average value of the PMM inductance: $L_{ave} = 0.5(L_d + L_q)$. Then, the critical i_q value can be derived as follows:

$$i_{qC} \approx \frac{R_s i_{d0}}{0.5 \omega_{re0} (L_d + L_q)} \tag{30}$$

Hence, under condition

$$|i_q| \le |i_{qC}| \tag{31}$$

k_{iv} should become negative in order to maintain stable operation. However, this is difficult for practical implementation since the critical value (30) depends on the machine parameters which can vary during significantly during operation.

The value of k_{iv} is proposed to be set adaptively to a half the boundary limit value k_{L4} (28):

$$k_{iv} = k_{L4}/2 \tag{32}$$

with k_{iv} maximum and minimum limits of 100 and 15.
According to criteria (27) this selection will guarantee stable operation if $k_{L3} > 0$. To satisfy the latter with some safety margin, I_{max} should be high enough so that the resultant i_q^* given by (9) is always larger than, for example, $2i_{qC}$. This condition can be formulated as follows:

$$I_{\max} > \sqrt{i_d^{*2} + (2i_{qC})^2} \tag{33}$$

Conditions (32) and (33) will guarantee stable operation in generation LM.
For UM, the range of k_{iv} for stable operation at 3600 rpm is calculated as well as illustrated by Fig. 11. It is to be noted that k_{iv} is always positive and can be set as high as possible for generating mode operation. In motoring mode the limit decreases with the increase in i_q. However, this limit is high enough to allow for k_{iv} gain to be selected such that good dynamic performance of the voltage control loop is achieved.

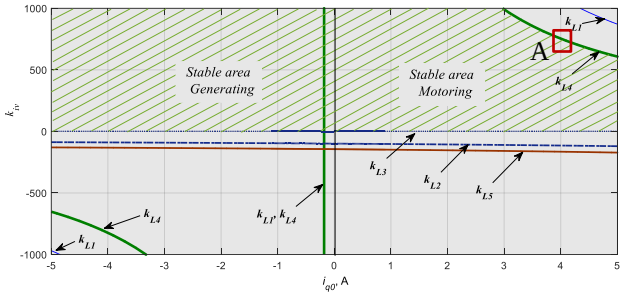

Fig. 11. k_{iv} range for stable UM operation.

V. Modified Current Limiting Strategy

The analysis in the previous section shows that the voltage control loop in generating LM is unstable if the machine i_q current is less than the critical value given by (30). This effect can also be explained as a natural result of the i_q^* limitation (9): according to the small-signal model (18) the i_q^* rate of change with respect to the change in i_d^* increases and goes to infinity when i_q^* approaches zero:

$$\lim_{i_{q-ref} \to 0} \frac{\Delta i_{q-ref}}{\Delta i_{d-ref}} = \infty \tag{34}$$

As this ratio can be considered as an open-loop gain for the voltage control in limiting mode (non-minimum phase plant, Section III.B), the high open-loop gain leads to instability (illustrated by the Root Locus in Fig. 9). The high value of $\Delta i_{q\text{-}ref}/\Delta i_{d\text{-}ref}$ causes the unstable area as illustrated in Fig. 10.

It is therefore proposed to modify the traditional current limiting model (3) such that the value of $\Delta i_{q\text{-}ref}/\Delta i_{d\text{-}ref}$ at small i_q in GM is limited. This is a novel addition to the conventional FW control strategy. The proposed modified current limiting trajectory is illustrated in Fig. 12.
The modified current limiting trajectory is linear and characterised the angle ϕ and I_{max}. The angle ϕ defines the angular position of the PMM current vector at which the modified limiter is enabled and circle i_q^* limit trajectory (9) is replaced by a linear one. In this study ϕ is selected such that i_q^* is a doubled i_{qC} value (30) to give a sufficient margin for the control system to switch the limiting trajectory before reaching the unstable area shown in Fig. 10. Hence, from (28), (32) and Fig. 9, one can derive:

$$\tan(\phi) = \frac{4R_s}{\omega_{re}(L_d + L_q)} \tag{35}$$

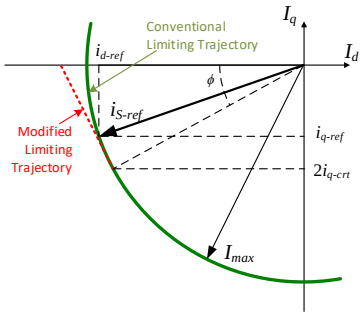

Fig. 12. Modified current limiting trajectory.

The analytical expression for the modified trajectory can be found from trigonometry of triangles in Fig. 12 as follows:

$$i_q^* = -\frac{I_{max}}{\sin(\phi)} - i_d^* \tan^{-1}(\phi) \tag{36}$$

Hence the small-signal model the new limiting trajectory can be presented by:

$$\frac{\Delta i_q^*}{\Delta i_d^*} = -\tan^{-1}(\phi) \tag{37}$$

which is a constant value for a given machine speed.
It should be noted that the modified current trajectory may yield a stator current magnitude higher than I_{max}, as can be seen from Fig. 12. This small increase over I_{max} (< 5%) can be mitigated in practical systems by monitoring the temperature of the PMM/converter and reducing I_{max} accordingly if necessary. This will maintain the thermal limit of the system.
The k_{iv} boundary limit k_{L4} (28) at different speeds is illustrated in Fig. 13 for conventional current limitation (9). Fig. 14 shows the same limit when the modified current limiting trajectory is introduced. It is clearly seen that this novel technique has a crucial stabilising effect on system response.

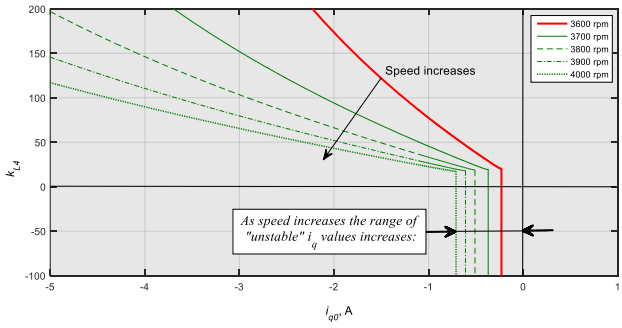

Fig. 13. Unstable area in limited i_q and generating mode using the current limiting model (3) only.

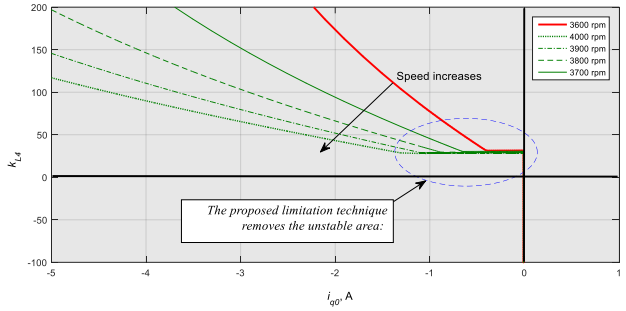

Fig. 14. Stabilisation effect of the modified current limiter (37).

As it can be seen from Fig. 13, the unstable area of operation expands as speed increases. The crucial effect of the proposed current limitation technique is illustrated by Fig. 14 where the unstable area is completely eliminated. Fig. 15 also shows the effect of the proposed limitation technique on the zero of the open loop transfer function of the voltage magnitude control given in (20). The proposed current limiter modifies the zero to remain in the right hand side of the s-plane during the unstable area until the PMM changes the operating mode from generating to motoring. Fig. 15 shows an example of zero modification against i_q at 3600 rpm speed.

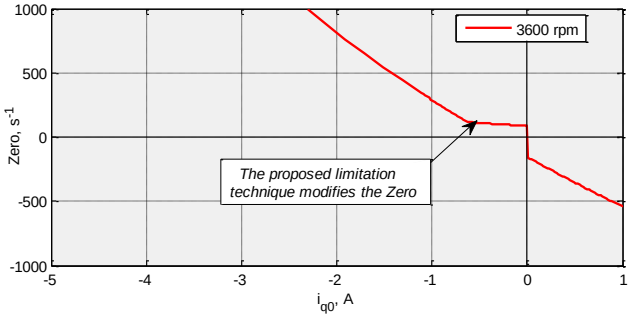

Fig. 15. The trajectory of the zero of the TF $\Delta V_s/\Delta i_d$ (20) for LM and applying the modified current limiter (37) .

Analysis of the SG system for a business jet application, as given in Appendix I, and designed for nominal power of 45kW at maximum speed of 32000 rpm shows that the unstable region for generating LM is up to 0.1 pu of the nominal power at the maximum operating speed. The parameters of the system at the nominal power and the maximum speed are: T_e = 13.4 Nm, i_q = 90.2 A, R_s = 53 mΩ and L_d = 100 μH. From (17) i_q^0 at the stability break-up point is 9.3 A, which is around 10% of the i_q at the nominal power and the maximum speed.

Summarising the theoretical part of the paper, the small-signal analysis and flux-weakening control design for PMMs is presented. The key findings of these analytical studies are as follows:

- It is shown that for PMM-based starter/generator (or more widely, for 2-quadrant PMM drive system) operated in unlimited i_q mode (UM) the plant of flux-weakening control loop changes from a non-minimum phase in motoring mode to a minimum phase in generating mode. Hence, a careful design of flux-weakening control is required in order to achieve stable operation across both generating and motoring modes. An integral controller is a suitable solution and its gain k_{iv} can be selected within a wide range.
- If the system is operated in generation mode and goes into i_q limitation (LM), then the flux weakening control loop become unstable for i_q values less than the critical value i_{qC} defined by (30). It is shown that this area in standard control scheme always exists and its size depends on the machine speed and on the value of i_q.
- A modified current limitation technique is proposed to eliminate the instability of the voltage control loop during current limitation. This is achieved by the proposed adaptive adjustment of the controller gain k_{iv} – as a result, as it is demonstrated, the unstable area is completely eliminated.

The flow chart given in Fig. 16 gives description of the transition mechanism between different operating modes and the suitable settings for the adaptive gain k_{iv}.

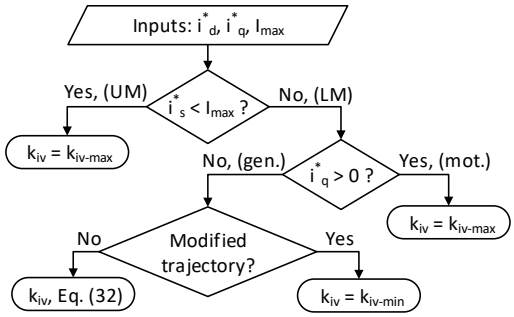

Fig. 16. Flow chart of transition between different operating modes in FW, $k_{iv\text{-}max}$ = 100, $k_{iv\text{-}min}$ = 15.

VI. Simulation Studies

This section will show some simulation results based on the S/G system with its designed controller. The first set of results show the control performance during the engine start-up phase when the PMM mainly operates as a motor. The torque-speed profile for the engine is based on Fig. 3 and has been adapted to suit the mock-up S/G system performance. It can be seen that the highest torque requirement is when the operating temperature is -40°C, therefore it is used for this simulation and the results are shown in Fig. 17.

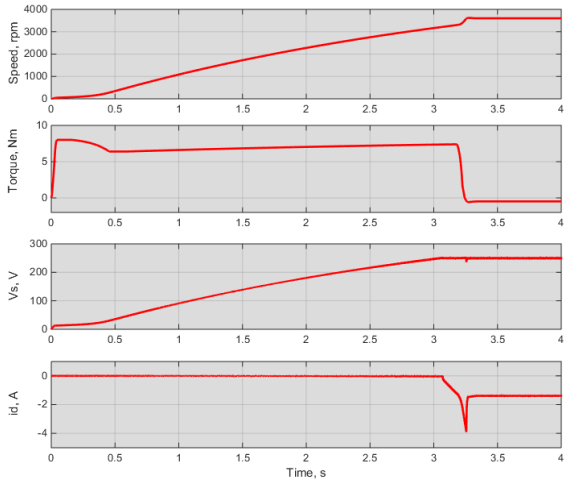

Fig. 17. Simulation results of S/G system in motoring mode with engine load torque profile

A speed reference of 3600rpm was set and it can be seen that the speed settled at t ~ 3.3s. The second graph shows the subjected load torque profile to represent the engine. V_s increased in proportion to the speed and was limited to 250V according to the FW controller reference value. This FW action is evidenced by non-zero i_d injected into the machine around the same time that V_s reaches 250V. After achieving the desired motoring speed, the engine goes into self-sustained mode and the torque changes sign as the machine goes into generation mode (t ~ 3.3s). This can be evidenced by the negative value of machine torque after t ~ 3.3s. This negative torque value is defined by the electrical loads. The k_{iv} for the FW controller was set to 100 as the operating condition was mainly in motoring LM. The results show that the designed FW controller is capable of supporting the S/G system in motoring mode where the engine start stage occurs.

Fig. 18 shows the operating conditions of the S/G system when transitioning between UM/LM, and generating/motoring in UM. For this example, I_{max} is fixed at 4A and the operating speed is 3600rpm.

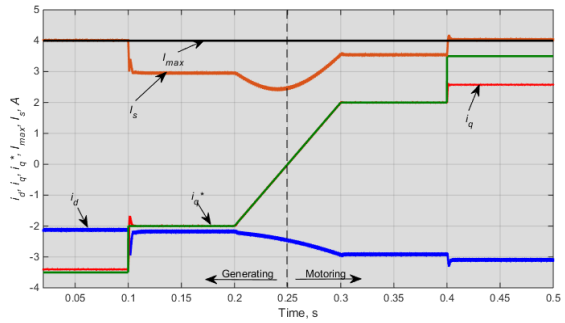

Fig. 18. Simulation results of S/G system at various operating conditions (Generating/motoring, UM/LM).

Before t = 0.1s, the S/G system is operating in LM, generating mode. This can be observed by the fact that the stator current, I_s, which is the magnitude vector of i_d and i_q is limited at I_{max} = 4A. Another indication is a small steady state error present between i_q and its reference value (i_q^* = -3.5A). At t = 0.1s, i_q^* is step changed to -2A and the operating mode transitions to UM, generating mode, where I_s is below the threshold of I_{max}. It is followed by a ramp change of i_q^* to +2A at t = 0.2s. This is done to show the smooth change from generating to motoring mode in UM. There is a step change of i_q^* to +3.5A at t = 0.4s to shift to LM, motoring mode. Throughout the change in operating modes, the FW controller works smoothly by providing the necessary i_d. This set of results show stable operation across generating/motoring in UM and UM/LM.

The next section shall deal with the experimental validation of the proposed FW controller.

VII. Experimental Investigation and Validation

As mentioned in Section V, experimental support to this study is provided using a small-scale test bed based on a 2.54kW PMM described in Appendix II. The validation of small-signal models, stability analysis and control design presented in the previous sections is reported in this section.

A. Validation of Stability Analysis

In this experiment, the stability boundaries for k_{iv} derived in the previous sections are validated in unlimited and limited i_q modes, respectively.

1) Motoring mode, unlimited i_q case

For unlimited i_q mode the derived k_{iv} stability limits are illustrated by Fig. 11 for operation at 3600 rpm (1.05pu) with i_q^* =4A (0.5pu) and voltage reference 250V. The test scenario assumes operation close to point A as shown in Fig. 11.Theoretically this limit is approximately 750. However, in practice when k_{iv} was set to 650 and then changed to 700 the system became unstable. As shown in Fig. 19, initially k_{iv} is set to 650, i.e. just below the stability boundary limit, followed by step change to 700. The experimental results in Fig. 19 clearly demonstrate that the system exhibits instability when k_{iv} is increased (at t~0.422s). Hence, the analytically derived boundaries as shown in Fig. 11 and the non-minimum phase behaviour of the flux-weakening control loop in motoring UM are confirmed.

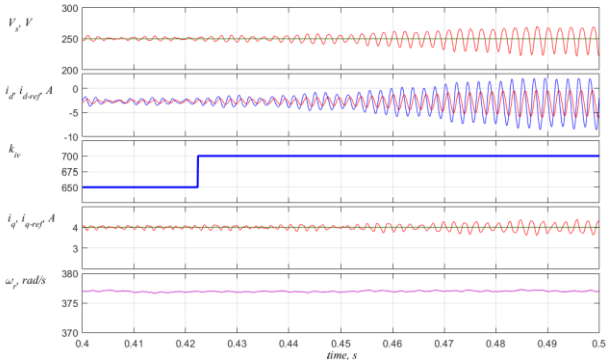

Fig. 19. Experimental validation of k_{iv} stability limit for motoring UM operation.

2) Generating mode, unlimited i_q case

This test confirms that in generation mode, with unlimited i_q, the voltage loop is minimum phase as derived in (16) and that there are no limits on k_{iv} from a stability point of view. The i_q^* was set to the same value as in the previous test, but for generating mode ($i_q^* = -4A$). The controller gain k_{iv} was initially set to 100 and then increased to 1000. The experimental results are reported in Fig. 20 and one can clearly see that the voltage control remains stable. Hence, the small-signal analysis reported by Fig. 11 and a minimum phase property of the control loop are confirmed.

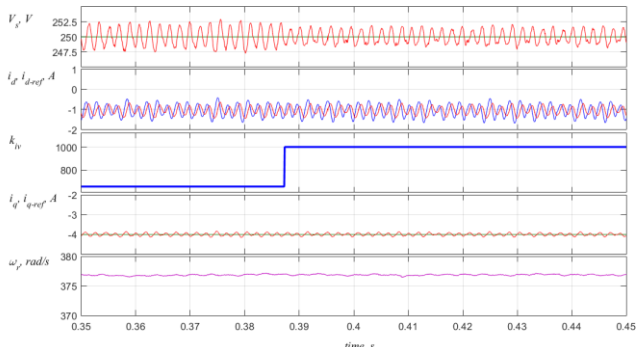

Fig. 20. Experimental validation of k_{iv} stability limit for unlimited i_q and generating mode of operation.

3) Motoring mode, limited i_q case

The test was repeated under motoring mode with $i_{q\text{-ref}}$ = 4 A. The gain k_{iv} was changed from 100 to 1000. The obtained test results are shown in Fig. 21. It can be seen that the system operates stably after the change of k_{iv} to 1000. This again experimentally confirms the minimum phase behaviour of the voltage control loop in limited i_q and motoring mode.

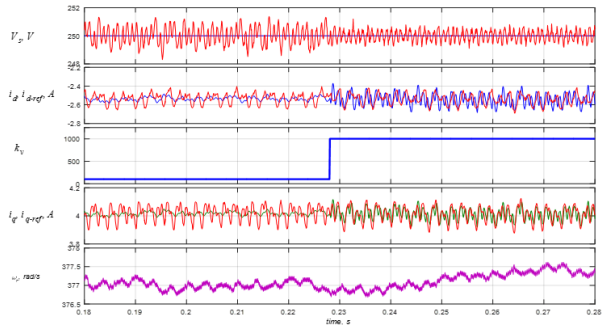

Fig. 21. Experimental validation of stable operation in motoring LM operation

4) Generating mode, limited i_q case

In this test, the stability boundary limits for k_{iv} for LM generating operation in Fig. 10 are validated. During this test, the machine was operated in the vicinity of point B as shown in Fig. 10 (3600rpm, voltage reference 250V). The current limit I_{max} is set to 4.5A according to (9) which results in i_q^* = -4A. The voltage controller gain k_{iv} is first set to 400 and then changed to 550 in order to exceed the limit k_{L4} defined by (28). Theoretically this limit is approximately 530. In practice, when k_{iv} was set stepped to 550 the system became unstable. The experimental results are reported in Fig. 22 from which it is clearly seen that the voltage control becomes unstable after increase of k_{iv} at t~0.544s. Hence, the analytical result for stability boundary in this operation mode is confirmed.

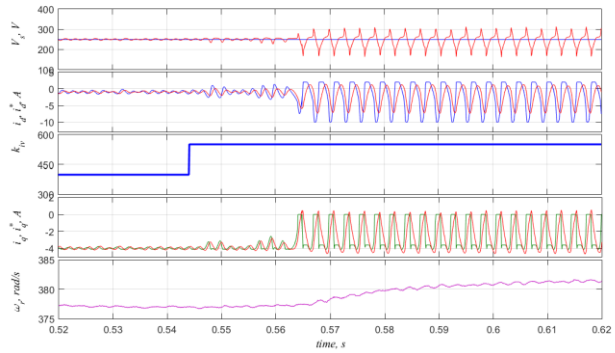

Fig. 22. Experimental validation of k_{iv} stability limit for generating LM.

B. Validation of the proposed current limiting technique

This test was carried out to validate the effectiveness of the proposed current limiting method (36) for elimination of the unstable area of operation shown in Fig. 13. The test started with PMM operation in generating LM at 3700 rpm (1.08pu) using traditional current limitation (9). I_{max} was set to 1.7A (~0.2pu) in order to place the PMM operating point within the unstable area shown in Fig. 13. The controller gain k_{iv} was set to the minimum limit which is equal to 15. The experiment results are reported in Fig. 23. It can be seen that in these conditions (before t~0.7s) the voltage control was unstable. At t~0.7s the modified current limit (36) was introduced and the voltage control loop stabilises. One should also note that i_q^* stabilises at a small value ~ -0.3 A. This experimentally proves the effectiveness of the proposed current limiting method for stabilising the voltage loop at small loads.

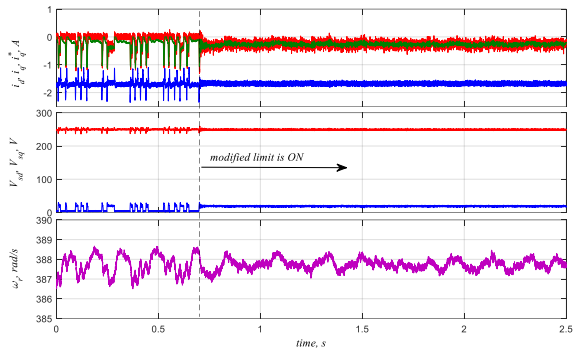

Fig. 23. Experimental results for validating the stability of the proposed modified current limit trajectory.

C. Validation of adaptive k_{iv} gain

The purpose of this test is to demonstrate the effectiveness of the proposed adaptive k_{iv} gain and modified current limiting (36) for establishing smooth transition from generating into motoring mode and for elimination of unstable operation area. At the beginning of the test, the PMM was operated at 3700rpm in generating mode with I_{max}=4A. Then, I_{max} was slowly decreased to 1.7A within 1s and remains fixed at 1.7A for a further 1s. Afterwards, the operating mode is changed to motoring (at t =2.3s) and I_{max} was gradually increased from 1.7A to 4.5A. The experimental results are shown in Fig. 24. It can be clearly seen that the voltage control was stable at the beginning of the test and becomes unstable when i_q reduces (if $|i_{q\text{-ref}}| < 2.3$A). This agrees with the k_{iv} boundary limits given in Fig. 13. Once the mode of operation is changed to motoring at t =2.3s, the voltage control stabilises.

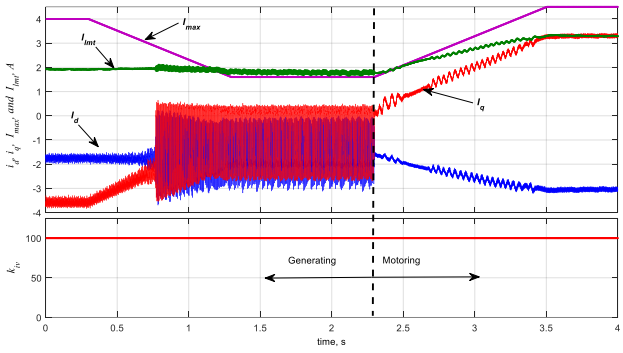

Fig. 24. Experimental validation of the need for adaptive k_{iv} in limited i_q and generating mode.

In the next test run, the adaptive controller gain k_{ivA} (32) was introduced. This was implemented using a lookup table to reduce the computational complexity of the control algorithm. The lookup table for k_{ivA} is mapped against the motor speed and i_q^*. The controller gain k_{iv} changes adaptively within the range from 15 to 100. The modified current limit (36) was enabled

when condition (33) is satisfied in generating LM. The transition from generating into motoring has been repeated under the same scenario as in previous run and the test results are reported in Fig. 25. The results show stable operation even at small current due to introduction of the proposed current limitation technique and adaptive updating of k_{iv}. The machine goes smoothly from generating into motoring mode.

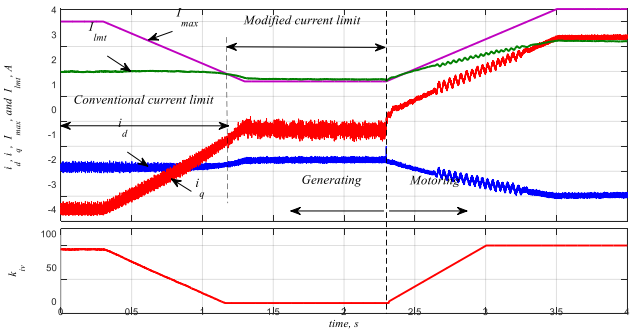

Fig. 25. Experimental investigation of modified current trajectory and adaptive k_{iv}.

Note that there are some oscillations in the i_d and i_q currents during the time period from t = 2.7s to t = 3.3s. These oscillations are due to disturbances originated from the DC drive controller during regenerative mode and have no link with the voltage control loop of the investigated PMM-based system.

The experimental results shown in Fig. 24 - Fig. 25 confirm the importance of using the adaptive k_{iv} and the modified current limit method to achieve stable voltage control in generating LM.

VIII. Conclusions

The paper has reported detailed, rigorous control analysis and design for a PMM based aircraft electric starter-generator operated in flux-weakening mode. It was found that the traditional flux weakening PMM control goes unstable if the machine is operated in generating mode with small i_q in current-limiting mode. This effect is explained by the high gradient of the circle-based current limiting trajectory traditionally used in PMM drives. A modified current limiting technique is proposed to limit the gradient value at small i_q values. The proposed approach is analytically proven to eliminate these unstable areas. In addition, an adaptive voltage controller is designed to achieve stable voltage control in generating mode irrespective of the machine operating point. The designed adaptive voltage controller with the modified current limiter guaranteed stable operation over both quadrants with smooth transition between various PMM operating modes.

This study was targeted at a particular application, namely, a PMM-based aircraft starter-generator system, however the results achieved may be valuable and important for design of wider class of electric drives, in particular, for two-quadrant PMM drives with frequent change between starting and generating regimes under current-limiting operation.

The analytical small signal based analysis and the proposed control design with the expected system performance were successfully verified and validated by experimental investigation.

IX. References

[1]. B. Bose, “Global energy scenario and impact of power electronics in 21st century,” Industrial Electronics, IEEE Transactions on, vol. 60, no. 7, pp. 2638–2651, July. 2013

[2]. I. Moir, and A. Seabridge, “Aircraft systems: Mechanical, electrical, and avionics subsystems integration”, John Wiley & Sons, 2008.

[3]. B. Sarlioglu and C. T. Morris, "More Electric Aircraft: Review, Challenges, and Opportunities for Commercial Transport Aircraft," IEEE Transactions on Transportation Electrification, vol. 1, pp. 54-64, 2015.

[4]. F. Gao, X. Zheng, S. Bozhko, C. I. Hill, and G. Asher, "Modal Analysis of a PMSG-Based DC Electrical Power System in the More Electric Aircraft Using Eigenvalues Sensitivity," IEEE Transactions on Transportation Electrification, vol. 1, pp. 65-76, 2015.

[5]. S. Bozhko, Y. Seang Shen, G. Fei, and C. Hill, "Aircraft starter-generator system based on permanent-magnet machine fed by active front-end rectifier," in Industrial Electronics Society, IECON 2014 - 40th Annual Conference of the IEEE, 2014, pp. 2958-2964.

[6]. I. Alan and T. A. Lipo, "Starter/generator employing resonant-converter-fed induction machine. II. Hardware prototype," *Aerospace and Electronic Systems, IEEE Transactions on*, vol. 36, pp. 1319-1329, 2000.

[7]. M. Hirst, A. McLoughlin, P. J. Norman, and S. J. Galloway, "Demonstrating the more electric engine: a step towards the power optimised aircraft," *Electric Power Applications, IET*, vol. 5, pp. 3-13, 2011.

[8]. W. Leonhard, "Adjustable-speed AC drives," in Proceedings of the IEEE, vol. 76, no. 4, pp. 455-471, Apr 1988

[9]. G. Gallegos-Lopez, et al., "Optimum torque control of permanent-magnet AC Machines in the field-weakened region," Industry Applications, IEEE Transactions on, vol. 41, pp. 1020-1028, 2005.

[10]. Ping-Yi and L. Yen-Shin, "Voltage Control Technique for the Extension of DC-Link Voltage Utilization of Finite-Speed SPMSM Drives," Industrial Electronics, IEEE Transactions on, vol. 59, pp. 3392-3402, 2012.

[11]. S. Jong-Hwan, et al., "A new robust SPMSM control to parameter variations in flux weakening region," in Industrial Electronics, Control, and Instrumentation, 1996., Proceedings of the 1996 IEEE IECON 22nd International Conference on, 1996, pp. 1193-1198 vol.2.

[12]. D. S. Maric, et al., "Two improved flux weakening schemes for surface mounted permanent magnet synchronous machine drives employing space vector modulation," in Industrial Electronics Society, 1998. IECON '98. Proceedings of the 24th Annual Conference of the IEEE, 1998, pp. 508-512 vol.1.

[13]. G. Xinhua, W. Xuhui, Z. Feng, S. Xuelei, and Z. Xingming, "PI parameter design of the flux weakening control for PMSM based on small signal and transfer function," in Electrical Machines and Systems, 2009. ICEMS 2009. International Conference on, 2009, pp. 1-6.

[14]. Rashed, M., Bozhko, S., Yeoh, S., Yang, T., Hill, C., “Flux Weakening Control of Permanent Magnet Electric Starter-Generator for Aircraft Applications,” in Power Electronics, Machines and Drives (PEMD 2016), 8th IET International Conference on.

[15]. Silverio Bolognani, Sandro Calligaro and Roberto Petrella, “Adaptive Flux-Weakening Controller for Interior Permanent Magnet Synchronous Motor Drives”, IEEE JOURNAL OF EMERGING AND SELECTED TOPICS IN POWER ELECTRONICS, VOL. 2, NO. 2, JUNE 2014, pp. 236-248.

[16]. N. Bedetti, S. Calligaro and R. Petrella, "Analytical design of flux-weakening voltage regulation loop in IPMSM drives," IEEE, Energy Conversion Congress and Exposition (ECCE), 2015.

[17]. S. Shinn-Ming, P. Ching-Tsai, and H. Yuan-Chuen, "A New Field-Weakening Control Scheme for Surface Mounted Permanent-Magnet Synchronous Motor Drives," in Industrial Electronics and Applications, 2007. ICIEA 2007. 2nd IEEE Conference on, 2007, pp. 1515-1520.

[18]. D. Stojan, D. Drevenšek, Z. Plantic, B. Grcar, and G. Štumberger, “Novel field-weakening control scheme for permanent-magnet synchronous machines based on voltage angle control,” IEEE Trans. Ind. Appl., vol. 48, no. 6, pp. 2390–2401, Nov./Dec. 2012.

[19]. L. Zhu, et al., "Deep field-weakening control of PMSMs for both motion and generation operation," in Electrical Machines and Systems (ICEMS), 2011 International Conference on, 2011, pp. 1-5.
[20]. T. Miyajima, H. Fujimoto, and M. Fujitsuna, "Model-based design of voltage phase controller for SPMSM in field-weakening region," in Applied Power Electronics Conference and Exposition (APEC), 2013 Twenty-Eighth Annual IEEE, 2013, pp. 2266-2272.
[21]. A. Damiano, G. Gatto, I. Marongiu, A. Serpi, and A. Perfetto, "A novel flux-weakening approach for Surface-Mounted Permanent Magnet Synchronous Machines," in Industrial Electronics Society, IECON 2013 - 39th Annual Conference of the IEEE, 2013, pp. 2547-2552.
[22]. R. Dutta, L. Chong, and M. F. Rahman, "Analysis of CPSR in motoring and generating modes of an IPM motor," in Electric Machines & Drives Conference (IEMDC), 2011 IEEE International, 2011, pp. 1474-1479.
[23]. J. Wai and T. M. Jahns, "A new control technique for achieving wide constant power speed operation with an interior PM alternator machine," in Industry Applications Conference, 2001. Thirty-Sixth IAS Annual Meeting. Conference Record of the 2001 IEEE, 2001, pp. 807-814 vol.2.
[24]. S. Shinn-Ming and P. Ching-Tsai, "Voltage-Constraint-Tracking-Based Field-Weakening Control of IPM Synchronous Motor Drives," Industrial Electronics, IEEE Transactions on, vol. 55, pp. 340-347, 2008.
[25]. P. Ching-Tsai and L. Jenn-Horng, "A robust field-weakening control strategy for surface-mounted permanent-magnet motor drives," Energy Conversion, IEEE Transactions on, vol. 20, pp. 701-709, 2005.
[26]. P. C.Krause, O. Wasynczuk, and S. D. Sudhoff, Analysis of electric machinery and dirve systems: Wiley-interscience, 2002.
[27]. M S. Morimoto, Y. Takeda, T. Hirasa, K. Taniguchi, "Expansion of operating limits for permanent magnet motor by current vector control considering inverter capacity", IEEE Trans. Industry Applications, vol.26, no.5, pp. 866-871, Sept./Oct. 1990.
[28]. A. Yazdani and R. Iravani, *Voltage-Sourced Converters in Power Systems*: John Wiley & Sons, Inc., 2010.

ACKNOWLEDGMENTS

The research reported in this paper has been funded from the European Community's 7th Framework Program (FP7/2007-2013) for the Clean Sky Joint Technology Initiative in a frame of AEGART project (grant agreement 296090), a part of EcoDesign ITD.

APPENDIX I. STARTER-GENERATOR SYSTEM PARAMETERS

S/G Parameters: P_{nom}= 45kW at 270VDC, nominal power; ω_{rn} = 8000rpm at 400Hz, nominal PMM speed; i_{rated} = 170A, rated current; f_s = 16kHz, sampling frequency; p_p = 3, the number of pole pairs; R_s = 53mΩ, stator winding resistance; L_d = 100µH, d-axis stator winding inductance; L_q = 100µH, q-axis stator winding inductance; ψ_r = 0.0333 Wb, magnet flux; J = 0.403 kg.m^2 , system inertia; K_m = 0.164, machine constant.
Control Parameters: k_{pid} = 0.87, i_d proportional current control gain; k_{iid} = 3908, i_d integral current control gain; k_{piq} = 0.87, i_q proportional current control gain; k_{iiq} = 3908, i_q integral current control gain.

APPENDIX II. MOCK-UP STARTER-GENERATOR SYSTEM FOR EXPERIMENTAL SUPPORT OF THIS STUDY

The PMM (Emerson, 115UMC300CACAA) is connected to a 2-level IGBT active front end converter built in-house and is controlled with a DSP (Texas Instrument, TMS320C6713 DSP Starter Kit) and FPGA board. The PMM is driven by a DC brushed machine (TT Electric, LAK 2100-A) using a commercial 4-quadrant DC drive (Sprint Electric, PLX 10) that acts as an active load (key converter/machine characteristics).
S/G Parameters: P_{nom}= 2.54kW, nominal power; ω_{rn} = 3400 rpm, nominal PMM speed; i_{rated} = 5A, rated current; f_s = 12.5kHz, sampling frequency; p_p = 3, the number of pole pairs; R_s = 1.25 Ω, the stator winding resistance; L_d = 6.17 mH, d-axis stator winding inductance; L_q = 8.38 mH, q-axis stator winding inductance; ψ_r = 0.23 Wb, magnet flux; J = 0.00115 kg.m^2 , system inertia; B_f = 0.0015 Nm.s, system friction constant; K_m = 4.5, machine constant.
Control Parameters: k_{pid} = 12.28, i_d proportional current control gain; k_{iid} = 8428.3, i_d integral current control gain; k_{piq} = 15.99, i_q proportional current control gain; k_{iiq} = 10724, i_q integral current control gain.

APPENDIX III. COEFFICIENTS OF THE TRANSFER FUNCTION (14)

$$a_0 = K_m\left(L_d - L_q\right)\left(v_{q0}\left(\psi_m + L_d i_{d0}\right) - v_{d0}L_q i_{q0}\right)i_{q0} - \left(R_s v_{d0} + L_d \omega_{re0} v_{q0}\right)T_{l0} ;$$

$$a_1 = -L_d v_{d0} + J\left(R_s v_{d0} + L_d v_{q0}\omega_{re0}\right) ; \quad a_2 = JL_d v_{d0} ; \quad b_0 = -T_{l0} ;$$

and $b_1 = J$.

APPENDIX IV. COEFFICIENTS OF THE TRANSFER FUNCTION (19)

$$a_{2L} = J\left(L_d i_{q0} v_{d0} - L_q i_{d0} v_{q0} T_{iqd}^{pi}\right);$$

$$a_{1L} = -i_{d0}T_{iqd}^{pi}\left(-T_{l0}L_q v_{q0} + J\left(R_s v_{q0} - L_q v_{d0}\omega_{re0}\right)\right) + i_{q0}\left(-T_{l0}L_d v_{d0} + J\left(R_s v_{d0} + L_d v_{q0}\omega_{re0}\right)\right);$$

$$a_{0L} = K_m\left(L_d - L_q\right)i_{q0}^2\left[v_{q0}\left(\psi_m + L_d i_{d0}\right) - v_{d0}L_q i_{q0}\right] - T_{l0}i_{q0}\left[R_s v_{d0} + L_d \omega_{re0} v_{q0}\right] - i_{d0}T_{iqd}^{pi}\begin{bmatrix} K_m\left(\psi_m + \left(L_d - L_q\right)i_{d0}\right)\left(\left(\psi_m + L_d i_{d0}\right)v_{q0} - L_q i_{q0} v_{d0}\right) \\ -T_{l0}\left(R_s v_{q0} - L_q v_{d0}\omega_{re0}\right) \end{bmatrix};$$

$b_{1L} = J$; $b_{0L} = -T_{l0}$; and $T_{iqd}^{pi} = \dfrac{T_{fiq}(s)}{T_{fid}(s)}$ is the ratio between the transfer functions of *q* and *d*- current control loops.